Command Shaping Applied to a Flexible Robot with Configuration-Dependent Resonance

Withit Chatlatanagulchai, Victor M. Beazel, and Peter H. Meckl, *Member, IEEE*

Abstract—**Joint flexibility is an intrinsic property in most industrial robot manipulators. Because of the great complexity of its model, the resonant frequencies of the two-link flexible-joint robot manipulator vary with the configuration of the manipulator. Our objective is to move the manipulator from point to point with the least amount of residual vibration at the end point in the shortest time possible. Two shaped command profiles, based on ramped sinusoidal basis function and segmented versine basis function, are compared against one another as well as against the unshaped bang-bang command profile. The segmented versine basis function was proved to be the most effective.**

I. Introduction

MANY dynamic systems are designed to be repositioned from one location or orientation to another in the shortest amount of time possible. For these systems, structural resonance will always be a limiting factor. Dampening structural resonance excited by the input is one way that has been employed. Another way, which includes command shaping method, is to shape the input to avoid exciting system resonant frequencies.

Aspinwall [1] was an early proponent of the use of basis functions to synthesize shaped commands for the motion control of flexible mechanism. Meckl [2], [3] later extended this approach. He performed a least-squares fit to one cycle of a square wave using an appropriately selected set of basis functions, subject to the constraint that the frequency content of the synthesized input command at the spectral locations of the system natural frequencies be minimized.

However, these open-loop command shaping techniques were developed for use with linear time-invariant flexible systems. In fact, reference [4] demonstrated that even a very simple nonlinear system, with a configuration-dependent natural frequency, could present a difficult challenge for input shaping methods.

Investigation of appropriate ways to extend these methods to systems with configuration-dependent resonance is still in its infancy. Some research, for example [4]-[7], was focused on training the parameters of an FIR filter to remove energy from the input to a system with configuration-dependent natural frequencies.

Joint flexibility exists in most robots. It arises from driving components such as actuators, gear teeth, or transmission belts. In some applications, the designers incorporate flexible joints into their products intentionally to absorb impact force and to reduce damage to the parts from accidental collision. The significance of taking the joint flexibility into account during the controller design process cannot be underestimated. The joint resonant frequencies, if omitted, can be excited and cause severe oscillations. The experiment in [8] confirmed that the designers should consider joint flexibility in both modeling and control design.

Applying the command shaping method to a flexible-joint robot manipulator has almost never been seen in the literature. Kinceler and Meckl [9] synthesized command functions to slew a two-link planar robot with flexible joints. The trajectory was subdivided into small enough pieces so that the natural frequencies of the system could be assumed to be constant on that interval. The equations of motion were linearized about the midpoint of each interval, and the eigenvalues for each linearized system were used to generate appropriate torques to traverse each interval.

The command shaping techniques used in this work are adapted from [10] and applied to the flexible robot dynamics with feedback control structure. We evaluate the effectiveness of various command profiles in reducing the residual vibration, and in reaching the end position in the shortest time possible. The command profiles are unshaped bang-bang profile, ramped sinusoidal basis function profile, and segmented versine basis function profile.

This paper is organized as follows. Section II presents the dynamics of the two-link flexible-joint robot. Section III provides some basics of command shaping method. Section IV discusses the feedback control structure. Section V details the command shaping method applied to the robot dynamics. Section VI presents conclusions.

II. Dynamics of the Two-Link Flexible-Joint Robot

We are interested in designing a point-to-point motion controller for the robot shown in Fig. 1. The objective is to have the least residual vibration at the final position as well as to finish the movement in the shortest time possible.

Manuscript received September 21, 2005.

W. Chatlatanagulchai and P. H. Meckl are with the Motion and Vibration Control Laboratory, School of Mechanical Engineering, Purdue University, West Lafayette, IN 47907-2088 USA (e-mail: chatlata@purdue.edu, meckl@purdue.edu; phone: 765-494-0539; fax: 765-494-5686).

V. M. Beazel is with the USAF Research Lab, Kirtland AFB, NM 87117 USA (e-mail: Victor.Beazel@kirtland.af.mil; phone: 505-853-7037; fax: 505-853-6151).

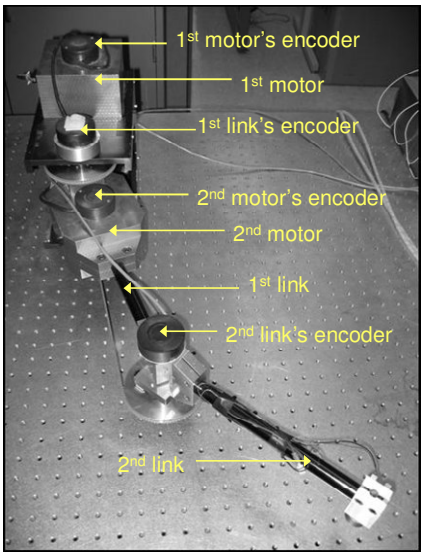

Fig. 1 Photograph of the two-link flexible-joint robot in our laboratory.

The robot operates in the horizontal plane, has two links and two motors. Input torque T_1 is applied to the first motor, which drives the first sprocket through a chain. The sprocket is attached to the first link via the first torsional spring that provides joint flexibility. The second motor is situated on the first link. Input torque T_2 is applied to the second motor which drives the second sprocket. The second sprocket is attached to the second link via the second torsional spring. Note that the torque does not directly drive the link, instead the link dynamics follow the dynamics of the torsional spring.

Let $\theta_1, \theta_2, \theta_3$, and θ_4 be the first-link angular position, the second-link angular position, the first-motor angular position, and the second-motor angular position, respectively. The equations of motion of this robot can be derived using the Euler-Lagrange method. Reference [11] has the details of the derivation of the equations of motion together with the details of the system identification.

III. Synthesis of Command Functions

Meckl [3] proposed a multi-objective cost function that minimizes the square of the difference between the synthesized command function and the bang-bang command function, while penalizing the magnitude of the Fourier transform in the spectral region of the natural frequencies of the system,

$$J_c = \underbrace{\frac{1}{T_f}\int_0^{T_f}\frac{1}{\tau_m^2}\left[f_r(t)-f_{cs}(t)\right]^2 dt}_{\text{Fit synthesized command profile to minimum time profile,}} + \underbrace{\rho\sum_{i=1}^{N}(\omega_i T_r)^2\left|F_{cs}^*(\omega_i T_f)\right|^2}_{\text{subject to attenuated spectral amplitude at modal frequencies.}}$$

where T_r is the system move time corresponding to a square wave or bang-bang input, T_f is the move time associated with a command shaped input, f_r is the bang-bang command profile used to move a rigid-body system in a time-optimal manner, f_{cs} is the command shaped profile, ω_i is the i^{th} natural frequency of the flexible system, ρ is the relative weighting between goodness of fit and the frequency domain penalty to be levied during the minimization process, τ_m is the maximum torque available, N is the number of frequencies around the nominal natural frequency ω_i, and F_{cs}^* is the Fourier transform of the dimensionless command shaped profile.

The partial derivatives of this cost function with respect to the basis function coefficients are then set equal to zero, and the resulting linear system of algebraic equations can then be solved for the coefficients of the command profile. The actual inputs to the routine that computes the coefficients of the shaped command profile are the vector of dimensionless natural frequencies, ωT_r, the number of terms to include in the command profile, L, and the relative weighting, ρ.

For systems that are not velocity limited, the basis functions suggested by Meckl [2] were ramped sinusoids possessing the following form:

$$f_{rs}(t) = \tau_m \sum_{k=1}^{L}\frac{\beta_k}{\alpha_k^2}\Phi_k^*(t)$$

where

$$\Phi_k^*(t) = \alpha_k\cdot\left(\frac{1}{2}-\frac{t}{T_f}\right)+\sin\left(\alpha_k\frac{t}{T_f}\right)-\frac{\alpha_k}{2}\cos\left(\alpha_k\frac{t}{T_f}\right) \qquad (1)$$

is the dimensionless ramped sinusoidal basis function, β_k is the coefficient of the k^{th} basis function, and α_k is a characteristic number associated with the k^{th} basis function. The characteristic numbers are selected so that the basis function has zero magnitude and slope at the endpoints. By using the boundary conditions, taking the time derivative of (1), and evaluating it at endpoints, the characteristic numbers must satisfy the equation

$$\frac{\alpha_k}{2}\sin\alpha_k+\cos\alpha_k-1=0,\ (\text{for } \alpha_k \neq 2\pi\text{n},\ \text{n} = 1,2,\ldots).$$

Another candidate is the versine basis function [12] having the form

$$f_{vs}(t) = \tau_m \sum_{k=1}^{L}\beta_k\Phi_k^*(t)$$

where

$$\Phi_k^*(t) = 1-\cos\left(\frac{2\pi k t}{T_p}\right),$$

and $T_p = \Delta v / a_m$ represents the time required to reach peak velocity, where Δv is the change in velocity and a_m is the maximum acceleration that the system can achieve. This basis function enables the acceleration of the system from one velocity state to a different velocity state.

IV. Feedback Control of the Robot Model

Fig. 2 shows the overall structure of the feedback control based on computed torque control law. The computed torque method partitions the control law into two portions, the model-based portion, which embeds a model of the system dynamics into the control law to make the system

behave in a linear fashion, and the servo-based portion, which controls the resulting linear behavior. This approach follows the work in [13]. The control gains should be selected so that the tracking error dynamics decay to zero in a well-behaved manner. $I_m = 1$ serves only to convert from units of acceleration to units of torque, and vice versa.

The overall torque contribution to the nonlinear system is given by

$$\tau = \hat{M}\left[\ddot{\theta}_d + k_v\left(\dot{\theta}_d - \dot{\theta}\right) + k_p\left(\theta_d - \theta\right)\right] + \hat{V} + \hat{C}\dot{\theta} + \hat{D} + \hat{K}\theta.$$

If the errors, $\dot{\theta}_d - \dot{\theta}$ and $\theta_d - \theta$, can be driven to zero, then $\ddot{\theta} = \ddot{\theta}_d$ will produce the necessary torque vector required by the nonlinear system to achieve the desired trajectory.

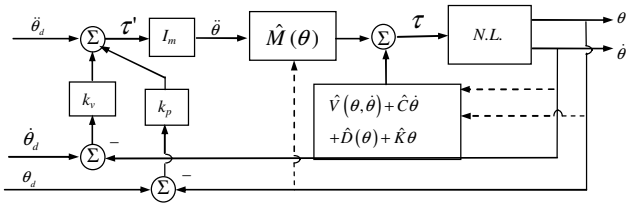

Fig. 2 Feedback control using computed torque method.

In Fig. 2, *N.L.* represents a truth model of the actual robot manipulator. $\hat{M}, \hat{V}, \hat{C}, \hat{D}$, and $\hat{K}$ are vectors and matrices that contain robot model parameters, where $\hat{M}$ is the inertia matrix, $\hat{V}$ is the coriolis and centrifugal vector, $\hat{C}$ is the viscous damping matrix, $\hat{D}$ is the Coulomb friction vector, and $\hat{K}$ is the spring stiffness matrix. Details of the robot model can be found in [11].

V. Command Shaping Applied to the Manipulator Dynamics via Feedback Control

In this section, we implement and compare three different command profiles. These command inputs were used to drive both links from a starting point to an endpoint. In all cases, both links were commanded to move from 0 to 1.25 radians.

In all cases, the robot manipulator model (indicated by $\hat{M}, \hat{V}, \hat{C}, \hat{D}$, and $\hat{K}$) was intentionally corrupted to have stiffness values 20% lower than the truth model to allow us to evaluate the robustness of the control system when subjected to model uncertainties. The controller gains for all cases were fixed at $k_v = 100$ and $k_p = 100$. The control input saturation limits are set at ± 1 *Nm.*

In open-loop systems, the standard command shaping approach takes a torque profile and approximates it with a set of basis function. In closed-loop systems, however, since the feedback variables are typically position and velocity variables, the torque profile is scaled by the average inertia to obtain a desired acceleration profile, and then, is integrated twice to obtain desired position and velocity profiles.

A. *Unshaped Bang-Bang Command Profile*

The model was first exposed to an unshaped bang-bang command profile. The dotted lines in Fig. 3a to Fig. 3f show the desired position, velocity, and acceleration profiles of the first and the second links. $\ddot{\theta}_{1d}$ and $\ddot{\theta}_{2d}$ possess the bang-bang profile. By integrating the acceleration profiles, we have the velocity and position profiles. The corresponding position, velocity, and acceleration profiles of the first and the second motors are then computed from the dynamic model.

Fig. 3g and Fig. 3h show the input torques to the first and the second motors. The solid lines in Fig. 3a to Fig. 3f show the actual output trajectories. Although the manipulator was able to achieve the steady-state angular positions, the large residual accelerations of the links at the end of the maneuver would have an adverse effect on pointing accuracy, making the early arrival of the links at their final orientation of little benefit.

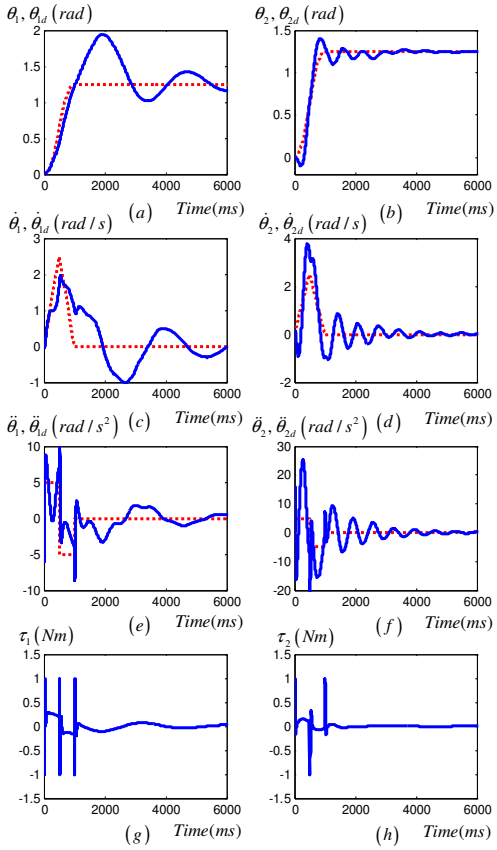

Fig. 3 Trajectories of both links in the unshaped case. Desired trajectories are in dotted lines. Actual outputs are in solid lines.

B. *Ramped Sinusoidal Basis Functions Command Profile*

Because the linearized natural frequency of the manipulator depends only on the relative angular position of the second link, θ_2, we linearize the closed-loop system in Fig. 2 around the operating points when θ_2 varies from -2 to 2 radians. The Simulink model of the closed-loop system is used with the Matlab command *linmod* to linearize the system and the Matlab command *damp* is used to compute the natural frequency as well as the damping ratio. The two dominant natural frequencies and damping

ratios are given in Fig. 4.

As shown by the acceleration outputs in Fig. 3e and Fig. 3f, the frequencies of the residual vibrations of the first and the second links follow the first mode and the second mode, respectively.

From the result in Fig. 4, the average natural frequency of the first mode, corresponding to the movement of the second link from 0 to 1.25 radians, is 2.4 rad/s whereas that of the second mode is 10.5 rad/s. We synthesized two commands from the ramped sinusoidal basis functions. The first command, used as the desired acceleration profile of the first link, was designed to have low spectral gain around 2.4 rad/s. The second command, used as the desired acceleration profile of the second link, was designed to have low spectral gain around 10.5 rad/s.

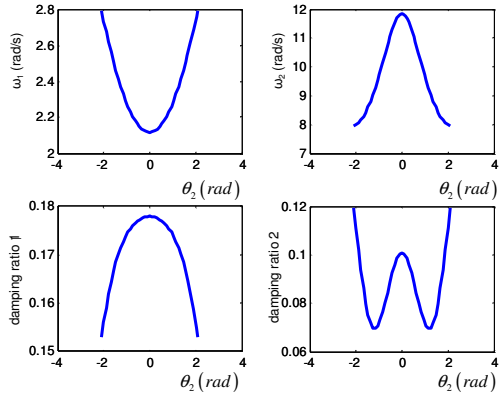

Fig. 4 Natural frequency and damping ratio of the closed-loop system with various second link positions, θ_2.

The following parameters were used to generate the shaped command profiles:

$$L = 10,\ \rho = 10,\ \omega_{n1} = 2\pi(2.4),\ \omega_{n2} = 2\pi(10.5),\ \tau_m = 5.$$

The spectral notch was extended by 20-percent in both directions around the nominal frequency to guarantee that all the unwanted energy in the region of the system resonant frequencies had been properly attenuated. The spectral magnitudes of both command profiles are given in Fig. 5.

After synthesizing the command profile using the ramped sinusoidal basis functions, the reference trajectory was next generated. The acceleration resulting from this command profile is

$$\ddot{\theta}_{rs}(t) = \ddot{\theta}_m \sum_{k=1}^{L} \frac{\beta_k}{\alpha_k^2} \Phi_k^*(t)$$

where $\ddot{\theta}_m$ is the maximum acceleration. The velocity and position profiles can be obtained from integrating the equation above.

The desired and output trajectories of both links, as well as the input torques, are given in Fig. 6. From Fig. 6e and Fig. 6f, the command profiles attenuate the residual vibrations quite well. The fact that some energy has been removed around the system resonant frequencies results in slower desired position trajectories as can be seen in Fig. 6a and Fig. 6b.

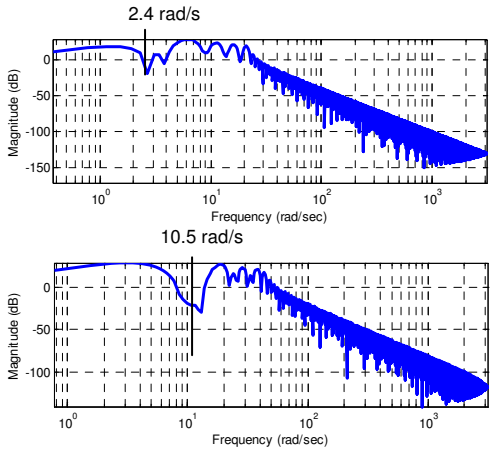

Fig. 5 Spectral magnitudes of both command profiles in the ramped sinusoidal case.

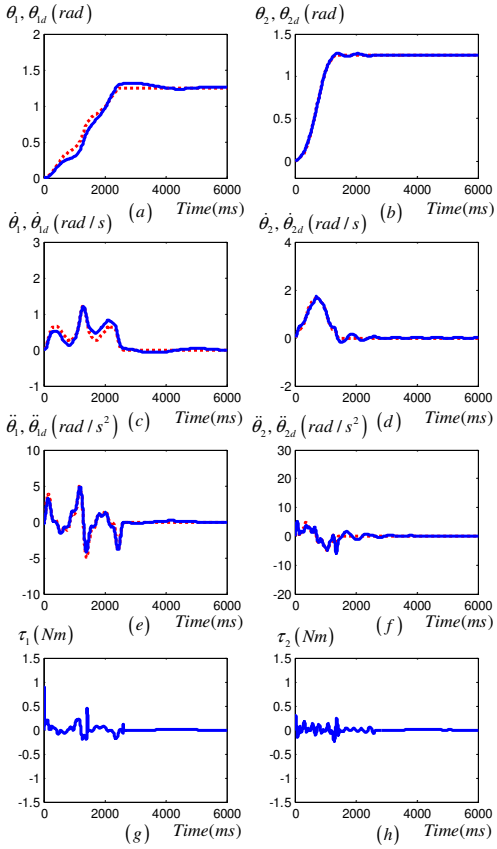

Fig. 6 Trajectories of both links in the ramped sinusoidal case. Desired trajectories are in dotted lines. Actual outputs are in solid lines.

C. Segmented Versine Basis Functions Command Profile

One of the drawbacks of using only one set of basis functions was that the attenuated region of the shaped command's frequency response had to be large enough to cover the whole range of resonant frequencies that the nonlinear system would encounter during a given maneuver. This broad-brush approach requires the unnecessary

omission of a lot of energy from the input that could otherwise be used to drive the system toward its final destination sooner.

The command shaping technique used in this section divides the trajectory into smaller pieces and then shapes each piece separately with its own set of basis functions. The versine basis functions can be used in situations where one or both of the endpoint velocities are non-zero.

The acceleration resulting from this command profile is analogous to the previous case, except that in this case, since there will be multiple segments, the maximum acceleration, $\ddot{\theta}_m$, was set equal to the average acceleration over each segment, that is, to the change in velocity divided by the time length of the segment,

$$\ddot{\theta}_{vs_i}(t) = \frac{\Delta\dot{\theta}_i}{T_{p_i}} \sum_{k=1}^{L} \beta_{i,k} \left[1 - \cos\left(\frac{2\pi k t}{T_{p_i}} \right) \right]. \qquad (2)$$

The maximum acceleration was thus selected to ensure that the states at the various segment boundaries match one another.

The velocity and position profiles can be obtained from integrating the equation above. After the segment components are computed, each segment position, velocity, and acceleration is concatenated with its predecessor to form the entire trajectory.

The trajectory is segmented at the time steps when the closed-loop natural frequency, as a function of θ_2, changes by a pre-specified Δf. The details of the trajectory segmentation process as well as some other requirements are extensively discussed in [10]. The resulting segmentations for the first and the second links are shown in Fig. 7a and Fig. 7b, respectively, where the X's are segment boundaries and the O's are segment freqencies. For the second link, the details of each segment including segment starting time, average frequency, initial position, initial velocity, and maximum acceleration scale factor are given in Table II.

Following the segmentation process, each of these segments was then shaped using the average frequency and the velocity information, and the following parameters:

$$L = 10,\ \rho = 3,\ \tau_m = 3.$$

Fig. 8 shows the spectral magnitudes of each segment for the second link. The command profile of each segment was then put together to form the desired acceleration profile. The desired position and velocity profiles are obtained from integrating (2).

The desired and output trajectories of both links, as well as the input torques, are given in Fig. 9. The command profiles attenuate the residual vibrations quite well, as shown in Fig. 9e and Fig. 9f. The fact that less energy is lost due to the locally shaping process results in faster desired position profiles. As shown in Fig. 9a and Fig. 9b, the first link and the second link each take 1.3 seconds to reach the end point (comparing with the ramped sinusoid case where the first link takes 2.4 seconds and the second link takes 1.5 seconds.)

D. Comparison of the Shaping Methods

Fig. 10 shows a comparison of the responses of the three command profiles. We can see from the unshaped responses that the residual vibration of the first link contains both a low-frequency component, corresponding to the first-mode natural frequency of the closed-loop system, and a high-frequency component, corresponding to the second-mode natural frequency of the closed-loop system. The residual vibration of the second link contains mainly the high-frequency component.

TABLE II
DETAILS OF EACH SEGMENT OF THE SEGMENTED VERSINE BASIS FUNCTION COMMAND PROFILE FOR THE SECOND LINK

Segment Number	Start Time (s)	Avg. Freq. (rad/s)	Init. Position (rad)	Init. Velocity (rad/s)	Max. Accel. Scale Factor
1	0.000	11.762	0.000	0.000	2.694
2	0.792	10.252	0.625	1.578	10.061
3	1.026	9.232	0.940	1.111	2.679
	1.582		1.250	0.000	

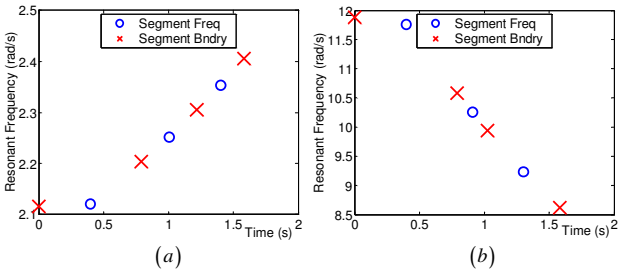

Fig. 7 The resulting segmentations for the first and the second link.

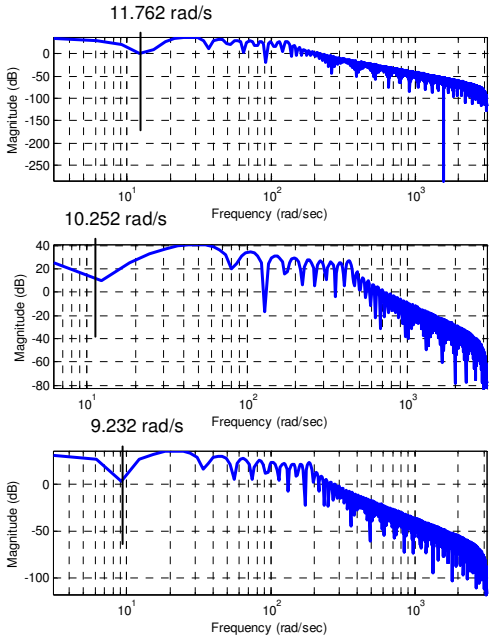

Fig. 8 The spectral magnitudes of each segment of the command profile for the second link.

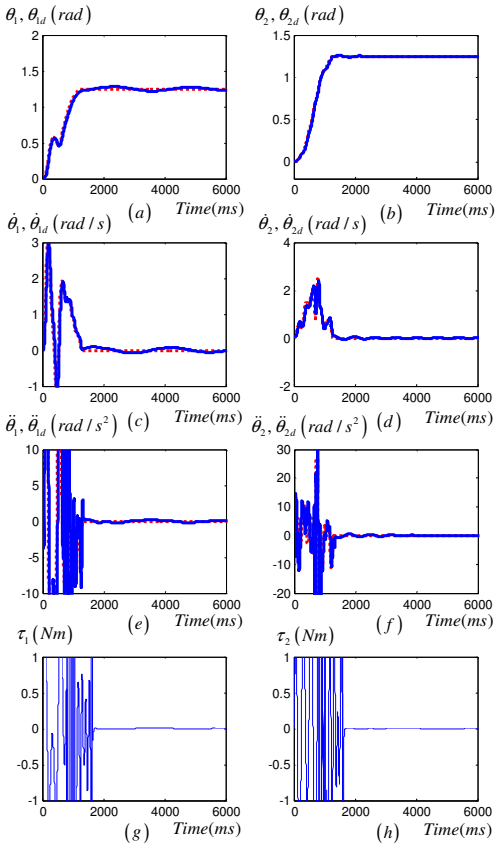

Fig. 9 Trajectories of both links in the segmented versine case. Desired trajectories are in dotted lines. Actual outputs are in solid lines.

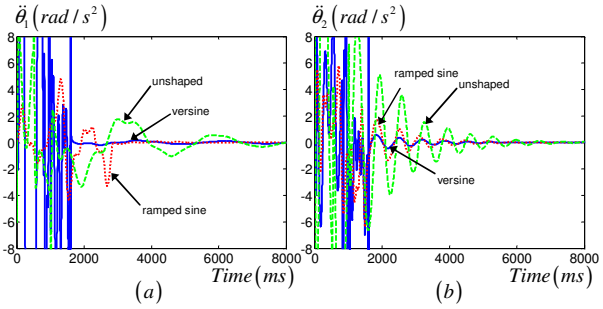

Fig. 10 Comparison of the acceleration outputs of the three profiles.

The command profiles from the ramped sinusoidal basis functions and the versine basis functions are equally effective in attenuating the residual vibrations of both links. However, since the segmentation process removes less energy, for a given maximum acceleration, the resulting desired position trajectories reach the endpoint faster than those of the ramped sinusoidal case. Therefore, the manipulator, following this faster trajectory, is able to reach the endpoint faster with similar amount of residual vibrations.

The controller may be more active in the segmented versine case as can be seen in Fig. 9g and Fig. 9h. However, this also depends on the values of the controller gains and the controller structure whose effects should be studied further.

VI. Conclusions

The command shaping based on segmented versine basis functions is an effective method for attenuating residual vibration during point-to-point maneuvering of a two-link flexible-joint robot.

Several issues arising from this work are worthy of further exploration. First, since the structure of the feedback control greatly influences the performance of the system, further investigation should be done to find a better structure that can accommodate the command shaping as well as handle the model uncertainties in a systematic way. Gain scheduling, H_∞-based design, or backstepping frameworks are some possible candidates. Second, experimental results are required to confirm that the command shaping method can indeed be successfully implemented on the flexible-joint robot.

References

[1] D. M. Aspinwall, "Acceleration profiles for minimizing residual response," *ASME Journal of Dynamic Systems, Measurement, and Control,* vol. 102, pp. 3-6, 1980.

[2] P. H. Meckl, "Minimizing residual vibration of a linear system using appropriately shaped forcing functions," S.M. thesis, Dept. Mechanical Eng., Massachusetts Institute of Technology, Cambridge, MA, 1984.

[3] P. H. Meckl, "Control of vibration in mechanical systems using shaped reference inputs," Ph.D. dissertation, Dept. Mechanical Eng., Massachusetts Institute of Technology, Cambridge, MA, 1988.

[4] K. Kozak, I. Ebert-Uphoff, and W. Singhose, "Locally linearized dynamic analysis of parallel manipulators and application of input shaping to reduce vibrations," *ASME Journal of Mechanical Design,* vol. 126, no. 1, pp. 156-168, 2004.

[5] J. Park, P. H. Chang, and E. Lee, "Can a time invariant input shaping technique eliminate residual vibrations of a LTV system?," *Proc. American Control Conference,* Anchorage, 2002, pp. 2292-2297.

[6] J. Park and P. H. Chang, "Learning input shaping technique for non-lti systems," *ASME Journal of Dynamic Systems, Measurement, and Control,* vol. 123, pp. 288-293, 2001.

[7] D. P. Magee and W. J. Book, "Optimal filtering to minimize the elastic behavior in serial link manipulators," *Proc. American Control Conference,* Philadelphia, PA, 1998, pp. 2637-2642.

[8] L. M. Sweet and M. C. Good, "Re-definition of the robot motion control problem: effects of plant dynamics drive system constraints, and user requirements," *Proc. of 23rd IEEE Conf. on Decision and Control*, Las Vegas, NV, 1984, pp. 724-731.

[9] R. Kinceler and P. H. Meckl, "Corrective input shaping for a flexible-joint manipulator," *Proc. American Control Conference,* Albuquerque, NM, 1997, pp. 1335-1339.

[10] V. M. Beazel, "Command shaping applied to nonlinear systems with configuration-dependent resonance," Ph.D. dissertation, Dept. Mechanical Eng., Purdue University, West Lafayette, IN, 2004.

[11] H. C. Nho, "Precise motion control of flexible-joint robot manipulators with an intelligent payload estimator," Ph.D. dissertation, Dept. Mechanical Eng., Purdue University, West Lafayette, IN, 2004.

[12] P. H. Meckl and W. P. Seering, "Controlling velocity-limited systems to reduce residual vibration," *Proc. 1988 IEEE Int'l Conf. on Robotics and Automation,* Philadelphia, PA, 1988, pp. 1428-1433.

[13] J. J. Craig, *Introduction to Robotics, Mechanics and Control.* California: Addison Wesley, 1986, pp. 224-237.